Arabian Journal of Chemistry (2019) **12**, 897–907

King Saud University

Arabian Journal of Chemistry

www.ksu.edu.sa
www.sciencedirect.com

ORIGINAL ARTICLE

A promising amendment for water splitters: Boosted oxygen evolution at a platinum, titanium oxide and manganese oxide hybrid catalyst

Islam M. Al-Akraa [a], **Takeo Ohsaka** [b,c], **Ahmad M. Mohammad** [d,*]

[a] *Department of Chemical Engineering, Faculty of Engineering, The British University in Egypt, Cairo 11837, Egypt*
[b] *Department of Electronic Chemistry, Interdisciplinary Graduate School of Science and Engineering, Tokyo Institute of Technology, Mail Box G1-5, 4259 Nagatsuta, Midori-ku, Yokohama 226-8502, Japan*
[c] *Research Institute for Engineering, Kanagawa University, 3-27-1 Rokkakubashi, Kanagawa-ku, Yokohama 221-8686, Japan*
[d] *Chemistry Department, Faculty of Science, Cairo University, Cairo 12613, Egypt*

Received 3 November 2018; accepted 22 January 2019
Available online 31 January 2019

KEYWORDS

Oxygen evolution reaction;
Electrocatalysis;
Spin-coating;
Titanium oxide;
Manganese oxide

Abstract A hybrid catalyst composed of a platinum thin layer and modified with manganese oxide (MnOx) is recommended for the oxygen evolution reaction (OER). The Pt layer of the catalyst was physically sputtered onto a TiOx-coated Si substrate (this TiOx layer was sputtered inbetween the Si substrate and Pt layer to improve their adhesion and prevent their mutual diffusion). On top of the Pt layer, another thin TiOx layer (~60 nm) was spun before the electrochemical deposition of MnOx. The investigation focused primarily to evaluate the impact of the catalyst's annealing in oxygen atmosphere on its catalytic activity toward OER. Interestingly, before the modification with MnOx, a large catalytic enhancement both in activity (~228 mV negative shift at 20 mA cm^{-2} if compared to conventional bare Pt catalysts) and stability was achieved at the catalyst annealed at 600 °C toward OER in 0.5 M KOH. Surprisingly, the addition of MnOx to the catalyst synergized a boosted activity amplifying the negative shift to 470 mV at the same current density. Bunch of materials and electrochemical techniques were combined to reveal important remarks about the catalyst's morphology, structure, composition and intrinsic activity which was attributed to electronic rather than geometric factors.

* Corresponding author.
E-mail addresses: islam.ahmed@bue.edu.eg (I.M. Al-Akraa), ohsaka@echem.titech.ac.jp, pt120866sa@kanagawa-u.ac.jp (T. Ohsaka), ammohammad@cu.edu.eg (A.M. Mohammad).
Peer review under responsibility of King Saud University.

ELSEVIER Production and hosting by Elsevier

1. Introduction

The climate change and the depletion of natural resources of energy have stimulated a great effort to sustain new convenient, efficient and green power supplies. In this regard, moving into renewability has become essential to fulfill desired life prosperity (Chakik et al., 2017; Xu et al., 2018a; Zhu et al.,

https://doi.org/10.1016/j.arabjc.2019.01.006
1878-5352

2018a). The concept of renewability should not stop at the production scale but extend to include the storage and transporting mechanisms. Actually, in order to save the inherent losses of electricity during transmission via long distance high voltage lines, the market is switched to distribute rather the electricity generators themselves. That necessitates storing the electricity obtained from renewable power plants in convenient chemical fuels which can be transported and converted again into electricity but on-site (El-Deab et al., 2015; Mohammad et al., 2015). Of the greenest methodologies of saving electricity, water electrolyzers were perfect as the saving mechanism would produce the cleanest carbon-free hydrogen fuel (Balogun et al., 2017; Park et al., 2018). Interestingly, the purity of hydrogen produced in proton exchange membrane (PEM) water electrolysis is as high as 99.999 vol% (Alfredo, 2012), which has made the process attractive for industrial fuel marketing (Chakik et al., 2017).

In order to optimize the chemical processes involved in water electrolyzers, not only the cathodic H_2 production, but also the anodic oxygen evolution reaction (OER) has to be considered (Balogun et al., 2016; Li et al., 2017; Zheng, 2017; Liu et al., 2018a; Liu et al., 2018c; Zhu et al., 2018b). In fact, OER is not only important for water electrolyzers but also for many other vital applications of energy conversion (Abdullah et al., 2009; Tahir et al., 2017) and energy storage technology (Beni et al., 1979; Tahir et al., 2017). Unfortunately, the OER reaction takes place in aqueous solutions at high potentials (> 1.5 V vs. RHE) where most metal surfaces are either dissolved or oxidized. Therefore, the development of a cheap, stable and efficient anode for this reaction deserves to be explored.

Several oxide-based materials have previously been proposed for OER. Among them, the oxides of cobalt (Osgood et al., 2016; Wang et al., 2018) and nickel (Sadiek et al., 2012; Han et al., 2015) have shown superiority. However, unfortunately, the quick instabilities of these oxides restricted their industrial applications. Although exhibiting a promising activity and stability (chemically and thermally), the oxides of noble metals such as ruthenium (Paoli et al., 2016) and iridium (Cherevko et al., 2016) were expensive. In fact, the catalytic activity of a given material toward a particular application depends not only on the material's nature but also on its synthetic protocol and perhaps the modification/contamination it may be subjected to (Mohammad et al., 2015). In some cases, the use of mixed oxides could result in synergetic effects improving the electrocatalytic activity, stability and selectivity of the electrode (Bagotsky, 2006; Pan et al., 2015; Guo et al., 2018; Liu et al., 2018b; Xu et al., 2018b). For example, the partial substitution of TiO_2 by CeO_2 in a RuO_2-based electrode material improved the electrocatalytic activity for OER but decreased the mechanical stability of the mixture (De Faria et al., 1996). This instability could be reduced by introducing a small amount of Nb_2O_5 to the electrode composition (Santana and De Faria, 2006). On the other hand, the modification of iridium oxide electrode with platinum nanoparticles resulted in an exceptional synergistic catalytic enhancement for OER (Yao et al., 2007). Alternatively, a negative potential shift of up to 100 mV in the onset potential of OER could be obtained on nickel nanoparticles-modified electrodes if compared with the reactivity of bulk Ni electrode (Cahen et al., 1981). Recently, a significant enhancement in the electrocatalytic activity of a platinum electrode for OER with a negative shift up to 300 mV in the onset potential of OER has been observed upon a modification with MnOx nanorods (El-Deab et al., 2007; Mohammad et al., 2008). In fact, titanium composites have been proposed as cheap materials in many industrial applications (Lee and Park, 2003; Li et al., 2006) and recently their oxides exhibited an enhanced catalysis for oxygen reduction (Mentus, 2004; Kim et al., 2007), water splitting (Nam and Han, 2007) and ozone production (Mohammad et al., 2009).

In this regard, several methods have been reported for the preparation of titanium oxide electrodes. These included the dry approaches such as sputtering (Takagi et al., 2001) and chemical vapor deposition (Battiston et al., 1994) and wet processes such as dip coating (Yoko et al., 1991), sol–gel (Selvaraj et al., 1992), spray coating (Wang et al., 1998) and spin-coating (Mohammad et al., 2007; Mohammad et al., 2009). Although easier and less expensive, wet methods often produce amorphous oxide film which requires further a post-annealing procedure to get a uniform oxide film with an acceptable structural characteristics (Koyama et al., 2006). The annealing condition was always important in determining the ratio of the different phases coexisting under certain conditions (Marino et al., 2004). The ratio of Ti^{4+} and Ti^{3+} contents in a TiOx/Pt catalyst was influenced as well by the annealing conditions in oxygen atmosphere (Boffa et al., 1995).

The purpose of this investigation resided in modifying an annealed spin-coated Si/TiOx/Pt/TiOx dimensionally stable anode with MnOx for applications in water electrolyzers. The electrode's activity and stability toward OER was investigated in solutions of different pHs. The influence of annealing conditions on the substrate's reactivity deserved a particular attention.

2. Experimental

2.1. Chemicals

All the solutions were prepared from chemicals (purchased from Wako Company, Osaka, Japan) of analytical grades using deionized water (a Milli-Q water system - Millipore, Japan). The N_2 gas employed in this investigation was also of a high purity.

2.2. Preparation and annealing of the substrate

The details of substrate's fabrication were previously outlined (Mohammad et al., 2009). For the sake of simplicity, the TiOx-coated Si substrate will be given the abbreviation "S". Shortly, the substrate's preparation involved a radio frequency (RF) sputtering (ULVAC, Inc., Methuen, MA, U.S.A) of a TiOx layer on a Si wafer at room temperature (RT) for 10 min under an RF power density of 6.4 Wcm^{-2} and a total gas pressure of 0.6 Pa (Ar/O_2 ratio = 0.48/0.52). The sputtering of this TiOx layer was intended to reinforce the Pt/Si adhesion and to control their mutual diffusion. The Pt layer was next sputtered (4.8 W/cm^2) onto the substrate (will next be abbreviated as S–Pt) at RT for 1 min under Ar atmosphere (0.7 Pa). The S–Pt electrode was next moved to a spin – coater (Kyowariken, K-359 S-1, Japan) to deposit a Ti (3%) metallic precursor (Koujundo Kagaku Co. Ltd., Japan) onto the topmost Pt layer. Two modes of spinning (1000 rpm for 10 s and at 3000 rpm for 30 s) were consecutively employed to deposit

the titanium precursor on the S–Pt electrode. The S–Pt/TiOx electrode was then left to dry for 10 min in air at RT and next at 200 °C for another 10 min. The average thickness of the Ti layer was ~60 nm. Next, the electrode was annealed in air for 10 min at different temperatures (500–850 °C).

2.3. Electrodeposition of manganese oxide

Manganese oxide (MnOx) was electrodeposited onto the S–Pt/TiOx electrode from 0.1 M Na_2SO_4 solution containing 0.1 M $Mn(CH_3COO)_2$ via cycling the potential between 0.0 and 0.4 V versus Ag/AgCl/KCl(sat.) at 20 mV s^{-1} for different number of potential cycles (Mohammad et al., 2018). Scheme 1 represents the preparation sequence of the the S–Pt/TiOx electrode up to the electrochemical modification with MnOx.

2.4. Electrochemical and materials characterization

The cyclic voltammograms (CVs, 0.1 V s^{-1}) and the linear sweep voltammograms (LSVs, 5 mV s^{-1}) were both measured in N_2-saturated (deoxygenated) 0.5 M H_2SO_4 using a BAS 100B/W electrochemical analyzer (Bioanalytical Systems, Inc, Indiana, USA). The working electrode and the counter (Pt spiral wire – ALS Co., Ltd, Tokyo, Japan) electrode were separated by a porous glass. The Ag/AgCl/KCl (sat.) electrode (ALS Co., Ltd, Tokyo, Japan) was used as a reference electrode. All potentials in this investigation, even if not mentioned, were measured against this reference. The real surface area of Pt in the electrode was determined based on the charge associated with the reduction of the Pt oxide layer (420 μC cm^{-2}) (Trasatti and Petrii, 1991).

The diffraction pattern and the crystal structure of the electrodes were obtained by grazing incidence X-ray diffraction (XRD) operated with Cu Kα (λ = 1.54056 Å) radiation at 45 kV and 360 mA (D8-DISCOVER, Bruker AXS, Billerica, Massachusetts, US). The morphology of the electrode and the surface mapping were captured by a scanning electron microscope (SEM: S-3400 NX Hitachi High-Tech Science Systems Corporation, Tokyo, Japan). An energy dispersive x-ray spectrometer (EDXS) was used to identify the elemental composition of the electrode.

3. Results and discussion

3.1. Effect of annealing

In the current study, the electrode is annealed at a range of temperatures (500–850 °C). Fig. 1 shows the different XRD spectra of the spin-coated S-Pt/TiOx as a function of their annealing temperature. The main peaks in the XRD patterns were tabulated (see Table 1) with their relative intensities which were calculated by normalizing the intensity of each peak against the highest available intensity (it corresponded to the anatase TiO_2 (1 0 1) up to 750 °C and to the rutile (1 1 0) at 850 °C). The dependence of the electrocatalytic activity of the electrode on the intensity ratio (degree of crystallinity) of the different crystallographic planes in the electrode might be possible. Analysis of the data in Table 1 reveals preserving the anatase structure for the electrodes annealed at temperatures up to 750 °C. A phase transformation from the anatase to rutile structure of the titanium oxide film is observed at 850 °C; in consistence with a previous report (Kim et al., 2007). The XRD data of the electrode annealed at 600 °C showed a particular pattern; it had the lowest peak intensity of the TiO_2 (anatase) (1 0 1) plane. In addition, the intensity ratios of the TiO_2 (anatase) (0 0 4) and (TiO_2) (anatase) (2 0 0) planes of this electrode were the highest among all the electrodes. This difference in the crystal structure of the electrodes may inspire a difference in their electrocatalytic activity toward OER.

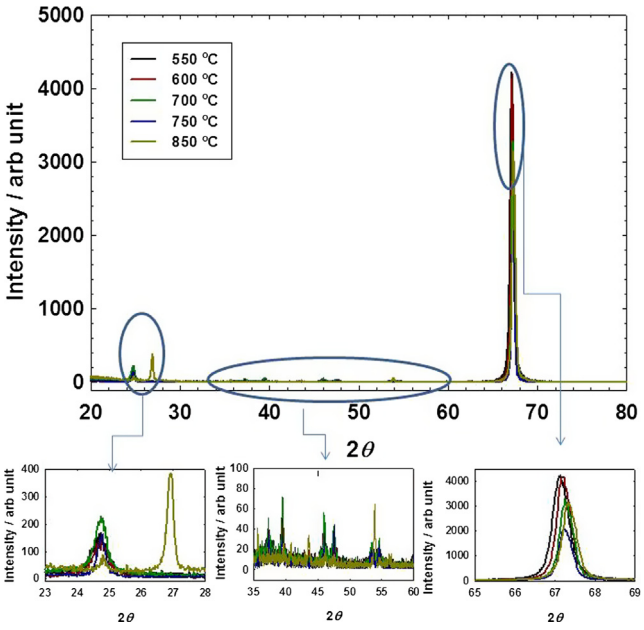

Fig. 1 XRD spectra of the spin-coated S-Pt/TiOx electrodes as a function of their annealing temperature.

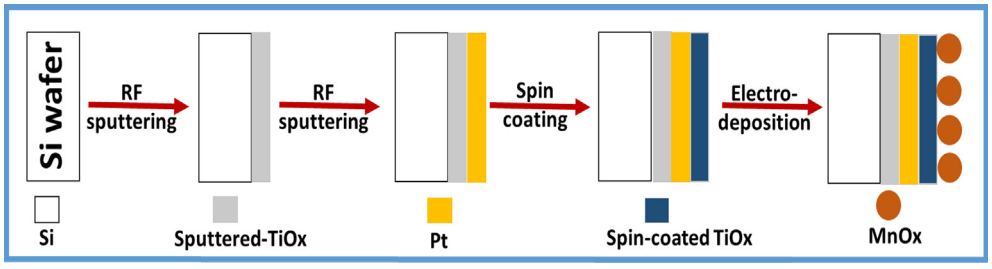

Scheme 1 Schematic representation for the preparation of the S-Pt/TiOx after modification with MnOx.

Table 1 The main peaks abstracted from the XRD patterns of the S-Pt/TiOx electrodes as a function of their annealing temperature. The relative intensity ratios (I%) of the different TiO_2 crystallographic planes are also included. To calculate these ratios, the intensity of each peak is normalized against the intensity of the TiO_2 (1 0 1) (up to 750 °C) and against the rutile (1 1 0) (at 850 °C). The reference data are taken from the international center for diffraction data, 2007.

Reference data				550 °C			600 °C			700 °C			750 °C			850 °C		
2θ	I	I%	Assignment	2θ	I	I%	2θ	I	I%	2θ	I	I%	2θ	I	I%	2θ	I	I%
24.77	999	**100**	Anatase (1 0 1)	24.74	169	**100**	24.7	143	**100**	24.74	229	**100**	24.72	146	**100**	24.82	90	–
27.24	999	**100**	Rutile (1 1 0)	–	–	–	–	–	–	–	–	–	–	–	–	26.94	387	**100**
35.81	612	**61**	Rutile (1 0 1)	–	–	–	–	–	–	–	–	–	–	–	–	35.62	41	**11**
37.38	194	**19**	Anatase (0 0 4)	37.26	39	**23**	37.36	39	**27**	37.24	51	**22**	37.3	38	**26**	–	–	–
39.76	100	**100**	Pt (1 1 1)	39.4	61	**100**	39.58	43	**100**	39.48	72	**100**	39.52	33	**100**	–	–	–
40.93	223	**22**	Rutile (1 1 1)	–	–	–	–	–	–	–	–	–	–	–	–	40.82	27	**7**
43.72	27	**0.027**	Rutile (2 1 0)	–	–	–	–	–	–	–	–	–	–	–	–	43.54	34	**9**
46.89	225	**22.5**	Anatase (2 0 0)	45.98	51	**30**	46.04	52	**36**	46.04	54	**24**	46.1	29	**20**	–	–	–
46.24	53	**53**	Pt (2 0 0)	47.48	34	**56**	47.48	31	**72**	47.58	45	**63**	47.54	27	**82**	–	–	–
53.90	488	**49**	Rutile (2 1 1)	–	–	–	–	–	–	–	–	–	–	–	–	53.88	64	**17**
67.45	31	**31**	Pt (2 2 0)	–	–	–	–	–	–	–	–	–	–	–	–	–	–	–

3.2. Effect of annealing temperature-electrochemical investigation

Cyclic voltammetry (CV), which is the potential-scan equivalent of double potential step chronoamperometry, has proven useful in obtaining information and acquiring qualitative information about fairly complicated electrochemical reactions (Bard and Faulkner, 2001; Wang, 2006). It has been successfully used in the characterization of supported VIII group metal catalysts (Tokarev et al., 2006). We have employed the CV's investigation to conveniently evaluate the electrochemical response of the electrodes, and to identify the location of redox potentials of the electroactive species in the electrochemical process. Fig. 2 shows a series of cyclic voltammograms (CVs; the current–potential curves resulted from the CV's investigation) for a bare Pt electrode (a) and different spin-coated S-Pt/TiOx electrodes annealed at 500 (b), 550 (c), 600 (d), 750 (e), and 850 °C (f). These CVs are all measured in 0.5 M H_2SO_4 solution under N_2 atmosphere at a potential scan rate of 0.1 V s^{-1}. All the CVs of Fig. 2(a–f) showed the characteristic behavior of a polycrystalline Pt electrode (Koryta et al., 1993). The potential pulse began at $E = -0.2$ V, where the electrode was covered with a layer of adsorbed hydrogen. When the potential was shifted to a more positive value, the adsorbed hydrogen was oxidized as two anodic peaks in the potential range from −0.2 to 0.1 V. These two peaks corresponded, in fact, to reactions at two different crystal facets: Pt (1 0 0) (lower potential) and Pt (1 1 1). Biasing the potential more positive up to 0.7 V inspired no faradaic processes and current was dedicated, solely, to charge the electrode's double-layer. At higher potentials ($E > 0.7$ V), the Pt surface was enriched with adsorbed oxygen and hydroxyl species in a process characterized by a drawn-out wave. Evolution of molecular oxygen started at a potential $E > 1.4$ V. Reversing the potential bias inspired opposite processes involving the PtO reduction and H_2 adsorption nearly at the same potentials of their corresponding anodic processes. However, Fig. 2, if carefully inspected, may infer more valuable information. For example, the appearance of the characteristic behavior of polycrystalline Pt electrode for all the S-Pt/TiOx electrodes (Fig. 2b–f) indicates that the spin-coated TiOx oxide layer was cracked. This cracked structure a little bit deviated the CV response of the S–Pt/TiOx electrodes (Fig. 2b–f) from the characteristic behavior of typical Pt substrates in acidic media. This deviation might become more significant if gas bubbles were accumulated within the cracks, particularly with the potential of the Pt/TiOx combination to support the H_2 spillover (Malevich et al., 1997). The charging current of the double layer increased at the S–Pt/TiOx electrodes if compared to the bare Pt electrode. This is actually expected with the deposition of the insulator titanium oxide film. The surface concentration of the adsorbed oxygen also increased at the S–Pt/TiOx electrodes which is desired for enhancing OER.

The electrocatalytic activity of the different electrodes toward OER was next inspected and analyzed in view of their annealing temperature. The LSVs of these electrodes were measured in N_2-saturated 0.5 M H_2SO_4 at a potential scan rate of 5 mV s^{-1}. One should realize the two important parameters addressing the electrode's activity toward OER; the position of the onset potential and the rate of OER. Moving the reaction toward a lower onset potential and a higher production rate is always desired to save energy. Fig. 3 shows a minor change in the catalytic activity toward OER for the electrode annealed at 500 °C (Fig. 3b) in comparison to that of the bare Pt substrate (Fig. 3a). Also, the electrodes annealed at 550 (Fig. 3c) and 750 °C (Fig. 3e) impeded more the OER both thermodynamically (by increasing its onset potential) and kinetically (by mitigating the rate of O_2 production). Interestingly, a noticeable enhancement for OER was observed for the two electrodes annealed at 600 and 850 °C. This enhancement appeared in a negative shift for OER of ca. −80 and −150 mV, respectively, for both electrodes if compared to that at the bare Pt electrode. This can save ultimately the electric power consumed to generate a given quantity of O_2 at a specified current. For example, to obtain a current density of 3 mA cm^{-2}, a potential of 1.824, 1.815, 1.893, 1.757, 1.948, and 1.734 V is required, respectively, with the bare Pt and the S–Pt/TiOx electrodes annealed at 500, 550, 600, 750 and 850 °C. We believe that the electrode' composition plays a vital role in the catalytic behavior of the electrodes. As previously discussed, the electrode annealed at 850 °C preserved a rutile structure which was previously recommended for OER (Santana and De Faria, 2006). Similarly,

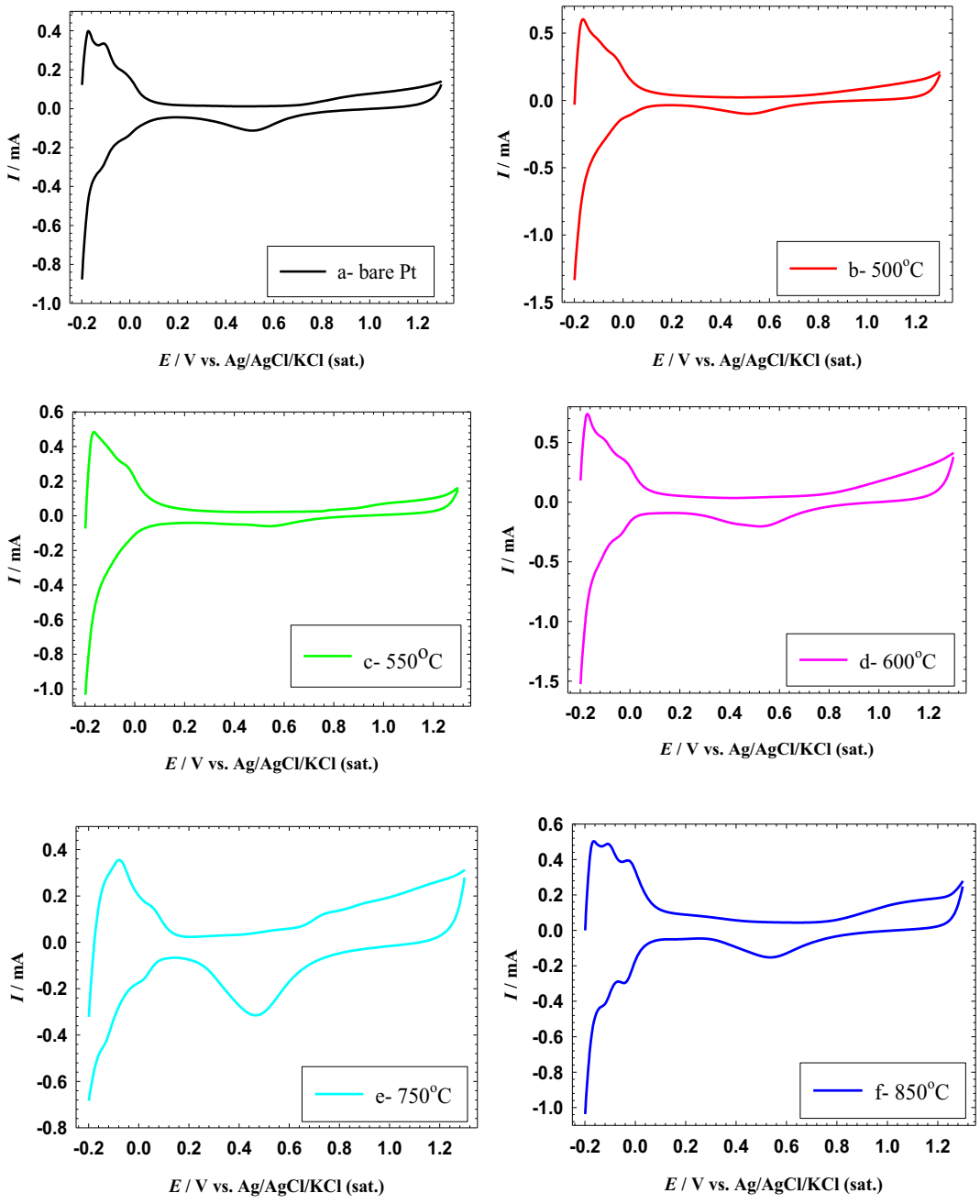

Fig. 2 The CVs obtained in N_2-saturated 0.5 M H_2SO_4 solution at a potential scan rate of 0.1 V s^{-1} for a bare-Pt electrode (a) and different spin-coated S-Pt/TiOx electrodes annealed at 500 (b), 550 (c), 600 (d), 750 (e) and 850 °C (f).

the particular XRD pattern observed for the electrode annealed at 600 °C is presumably behind the enhancement in its electrocatalytic activity. The rest of this investigation will deal primarily with the electrode annealed at 600 °C (S–Pt/TiOx(600)).

3.3. Effect of pH

Most of the work reported on OER has been carried out in either strongly acidic or strongly alkaline electrolytes according to the following equations:

$$2H_2O \leftrightarrow O_2 + 4H^+ + 4e \quad (1)$$

$$4OH^- \leftrightarrow O_2 + 2H_2O + 4e \quad (2)$$

Hence, the reaction is pH dependent and the electrolyte's composition in the close vicinity at the electrode's surface will be important. Fig. 4 depicts a comparison between the LSVs for OER obtained at the spin–coated S–Pt/TiOx(600) electrode and the bare-Pt electrode as a function of the electrolyte's pH. As clearly seen in Fig. 4, the S–Pt/TiOx(600) electrode showed an electrocatalytic enhancement for OER at all the pHs. This enhancement appeared in a cathodic shift in the onset poten-

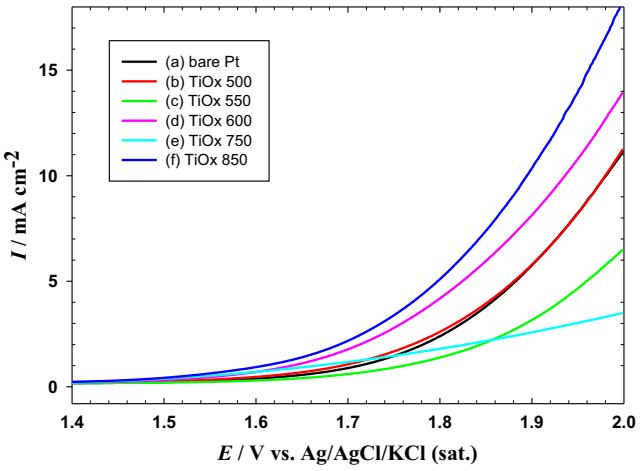

Fig. 3 LSVs for OER in N_2-saturated 0.5 M H_2SO_4 at a potential scan rate of 5 mV s^{-1} at the bare-Pt electrode (a) and spin-coated S-Pt/TiOx electrodes annealed at 500 (b), 550 (c), 600 (d), 750 (e) and 850 °C (f).

tial for OER while the degree of enhancement (the cathodic shift) depended to a great extent on the electrolyte's pH. A small shift in the onset potential for OER was obtained in 0.5 M H_2SO_4. A smaller shift is observed in a 0.1 M phosphate buffered solution (PBS, pH = 2.52), but the rate of OER was slower for the S–Pt/TiOx(600) electrode. The cathodic shift increased again gradually with the electrolyte's pH up to pH of 11.02, however, the rate of oxygen evolution did not change. In 0.5 M KOH, although the cathodic shift in the onset potential for OER was not the highest, an obvious increase in the rate of oxygen evolution is observed at the S–Pt/TiOx(600) electrode. In alkaline media, the faradaic current of OER at bare-Pt substrates did not increase smoothly with the potential; perhaps due to limitations of O_2 desorption at the electrode's surface. Fig. 4 also confirmed the fact that OER is pH dependent and is highly enhanced in alkaline media. The dependence of the catalytic enhancement for OER on the electrolyte's pH is displayed in Table 2. The catalytic enhancement is represented by the potential difference, $\Delta E = E_{bare\ Pt} - E_{spin\text{-}TiOx}$, required to generate the same current density for OER. Generally, the degree of enhancement was stronger in the basic than in acidic media. A maximum negative potential shift of 347 mV was obtained in 0.5 M KOH at 33 mA cm^{-2}.

3.4. Stability of the S-Pt/TiOx(600) electrode

The stability of the S-Pt/TiOx(600) electrode was then examined by measuring the LSV's curves before and after a continuous (for an hour) electrolysis experiment in 0.5 M KOH at 1 V. Fig. 5 exhibits a small positive potential shift in the onset potential of OER after the experiment. Interestingly, the two LSV curves before and after electrolysis were parallel (beyond 1.1 V), i.e., the electrode retained the same resistance for OER after the experiment.

3.5. MnOx-modification

The S-Pt/TiOx(600) electrode was next modified electrochemically with manganese oxide (MnOx). The MnOx was electrodeposited on the electrode from aqueous solution of 0.1 M Na_2SO_4 containing 0.1 M $Mn(CH_3COO)_2$ by applying 5, 15, 30 and 60 potential cycles between 0 and 0.4 V (vs. Ag/AgCl/KCl (sat.)) at 20 mV s^{-1}. The variation in the number of potential cycles during the electrodeposition of MnOx was carried out to investigate the influence of the MnOx's loading on the electrocatalytic performance of the electrode. The effective deposition of MnOx is confirmed electrochemically by inspecting the cyclic voltammograms obtained at the MnOx-modified electrodes in N_2-saturated 0.5 M H_2SO_4 (see Fig. 6). As obviously noticed in Fig. 6, the real surface area of Pt in the S-Pt/TiOx(600) electrode decreased with the MnOx's loading. One can, moreover, observe at potentials ($E > 0.6$ V), the tendency of oxygen adsorption decreases as the number of the potential cycle during the MnOx deposition increases. This probably occurred as a consequence of shrinking the accessible surface area of Pt with increasing the surface coverage of MnOx.

Morphologically, Fig. 7 depicts the homogeneous deposition of TiOx in a spongy porous texture on top of the S-Pt electrode (compare with the upper inset image "a" of the bare S-Pt/TiOx(600) electrode before MnOx-modification). The porosity permitted the accessibility of the electrolyte to the Pt surface. While MnOx was partially deposited onto the S-Pt/TiOx(600) electrode in aggregated microflakes (~3 μm in average size). In fact, MnOx is assumed to be deposited partially onto the Pt surface of the S-Pt/TiOx(600) electrode (refer to the shrinkage of the Pt active surface area in Fig. 6 with the MnOx deposition). The lower inset "b" of Fig. 7 shows the elemental mapping of Mn in the S-Pt/TiOx(600) electrode after electrodepositing MnOx (15 cycles). Interestingly, Mn was homogeneously distributed across the electrode, in agreement with a previous report (Bard and Faulkner, 2001). The MnOx (15 cycles) deposition at the S-Pt/TiOx(600) electrode was further confirmed by EDXS (Fig. 8) with a mass percent of 0.21 for Mn. This percent increased to 0.58 for the S-Pt/TiOx(600) electrode after electrodepositing MnOx (60 cycles).

To inspect the origin of the electrode activity, it is necessary to separate the electronic effect (related to oxide composition - true electrocatalysis) from the geometric effect (related to surface area) (Santana and De Faria, 2006). In our case, the deposition of MnOx resulted in a decrease in the accessible surface area of Pt. Therefore, the enhancement observed in the electrocatalytic activity of the electrode after its modification with MnOx is definitely attributed to an electronic rather than geometric effect.

The impact of the four different loadings of MnOx (corresponding to 5, 15, 30 and 60 cycles) on the electrocatalytic enhancement for OER was investigated by inspecting the LSVs (Fig. 9) for these MnOx-modified electrodes in N_2-saturated 0.5 M KOH. The current density was employed to exclude the influence of the geometric factor on the electrocatalytic activity of the electrodes. Interestingly, an obvious enhancement in the electrocatalytic activity for OER was observed after the electrodeposition of MnOx onto the S-Pt/TiOx(600) electrode. This enhancement appeared in a cathodic shift in the onset potential for OER. This cathodic shift in the onset potential for OER increased a little with the increase in the number of potential cycles employed in this investigation to electrodeposit MnOx. The enhancement appeared also in the potential required to sustain the same current density on the

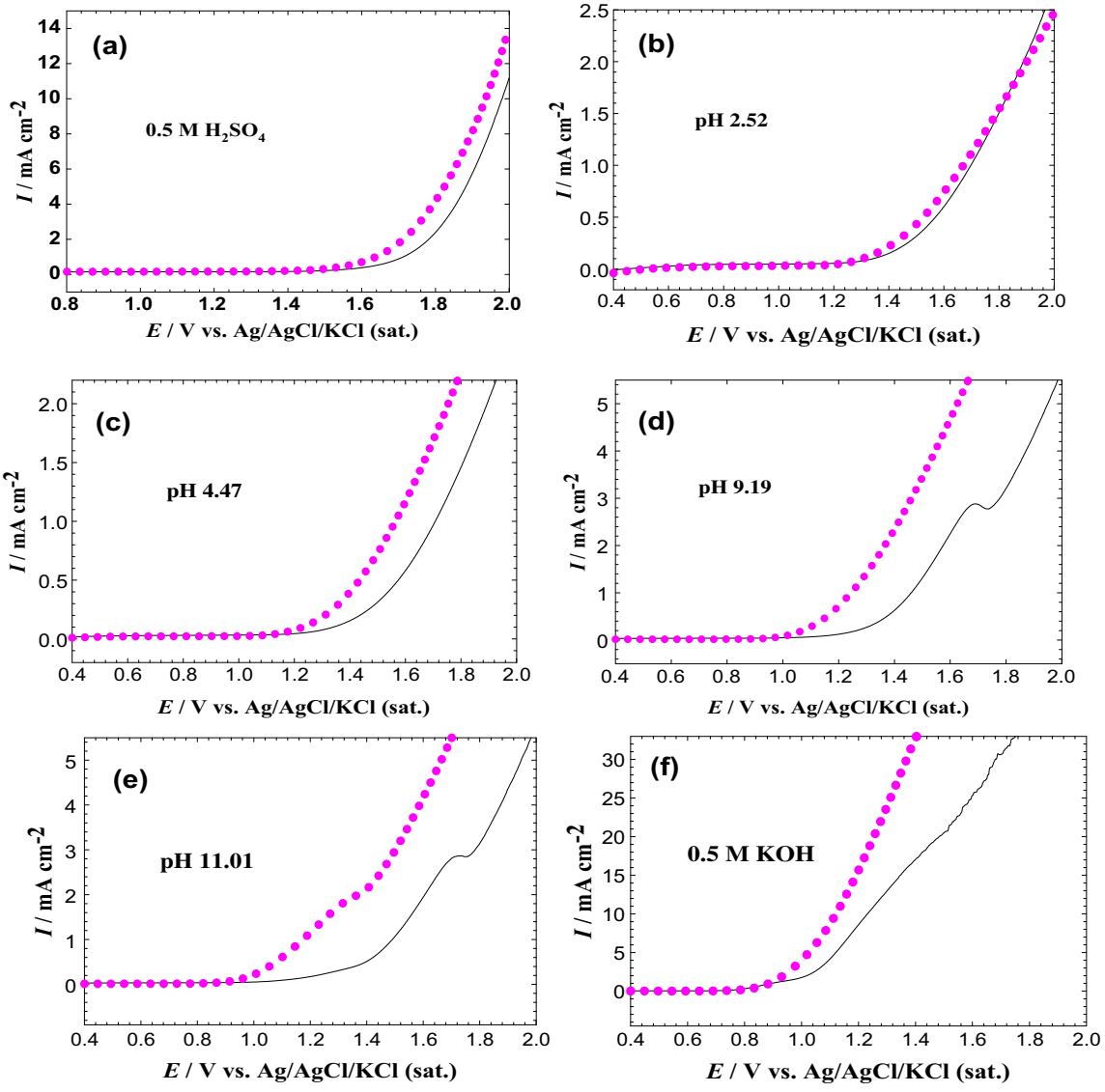

Fig. 4 LSVs response for OER at a potential scan rate of 5 mV s^{-1} for the bare-Pt electrode (solid lines) and the spin-coated S-Pt/TiOx electrode annealed at 600 °C (dotted lines) in N_2-saturated of 0.5 M H_2SO_4 (a), 0.1 M PBS (pHs 2.52, 4.47, 9.19, and 11.01) (b–e) and 0.5 M KOH (f) solutions.

Table 2 The potential difference (ΔE) for OER at the bare Pt and the S-Pt/TiOx (annealed at 600 °C) electrodes at variable current densities and electrolytes of different pHs. The potential difference (ΔE) represents the difference in the potential required to generate the same current density for OER ($\Delta E = E_{bare\ Pt} - E_{spin-TiOx}$) obtained at the bare Pt electrode and the S-Pt/TiOx electrode.

Current density, mA cm^{-2}	0.5 M H_2SO_4 ΔE (mV)	0.1 M PBS (pH = 2.52) ΔE (mV)	0.1 M PBS (pH = 4.47) ΔE (mV)	0.1 M PBS (pH = 9.19) ΔE (mV)	0.1 M PBS (pH = 11.01) ΔE (mV)	0.5 M KOH ΔE (mV)
1.0	74	27	143	215	317	6
2.0	69	−12	139	209	237	82
2.7	66	−50	–	215	209	93
5.0	58	–	–	324	275	95
11.0	43	–	–	–	–	118
20.0	–	–	–	–	–	228
30.0	–	–	–	–	–	311
33.0	–	–	–	–	–	347

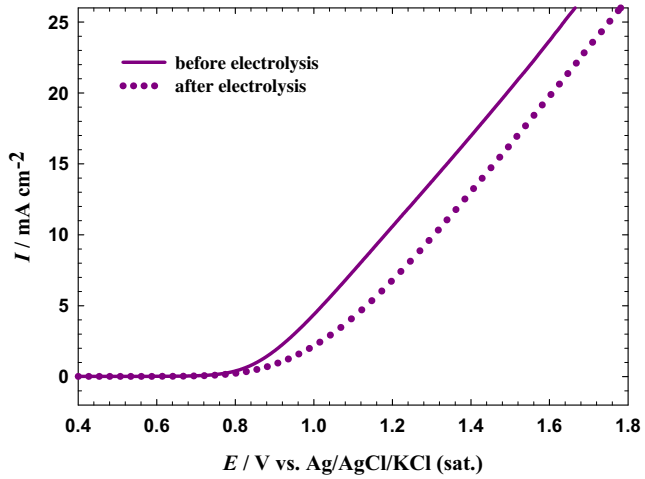

Fig. 5 The LSVs response for OER at a potential scan rate of 5 mV s^{-1} for the spin-coated S-Pt/TiOx electrode annealed at 600 °C in N_2-saturated 0.5 M KOH solution before (solid line) and after (dotted line) ~1 h of continuous electrolysis experiment in 0.5 M KOH at 1 V vs. Ag/AgCl/KCl (sat.).

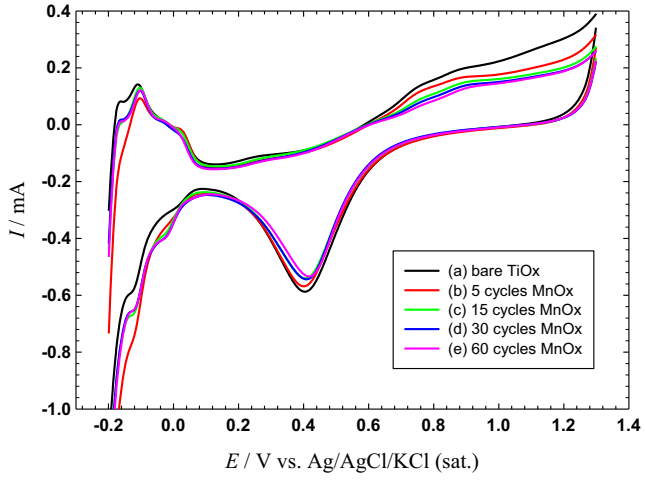

Fig. 6 The CVs obtained in N_2-saturated 0.5 M H_2SO_4 for the spin-coated S-Pt/TiOx electrode annealed at 600 °C before (a) and after modification with MnOx. The MnOx was electrochemically deposited from an aqueous solution of 0.1 M Na_2SO_4 containing 0.1 M $Mn(CH_3COO)_2$ by applying 5 (b), 15 (c), 30 (d), 60 (e) potential cycles between 0 and 0.4 V vs. Ag/AgCl/KCl (sat.) at potential scan rate of 20 mV s^{-1}.

different electrodes. For example, the potential required to obtain a current density of ~5.0 mA cm^{-2} changed from 1.057 V on the S-Pt/TiOx(600) electrode to 0.828 V after 5 cycles of MnOx deposition (i.e., 229 mV difference), to 0.791 V after 15 cycles of MnOx deposition (i.e., 266 mV difference), to 0.778 V after 30 cycles of MnOx deposition (i.e., 279 mV difference) and to 0.766 V after 60 cycles of MnOx deposition (291 mV difference). Fig. 9 also depicts that at potentials higher than 1.1 V, the enhancement achieved as a result of modifying the S-Pt/TiOx(600) electrode with MnOx (15 cycles) becomes better than that obtained if the electrode

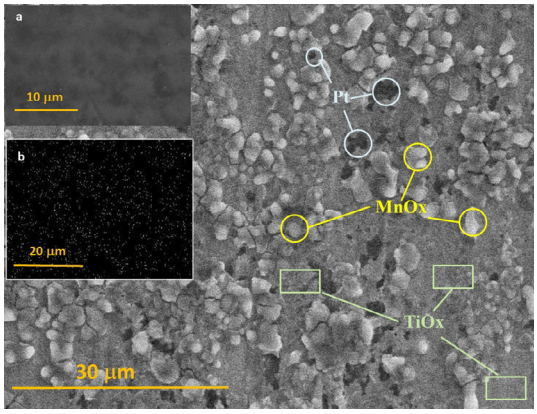

Fig. 7 The top-view SEM image of S-Pt/TiOx(600) electrode after modification with MnOx particles (15 potential cycles were employed in the deposition). The upper inset (a) is the bare S-Pt/TiOx(600) electrode before the MnOx-modification while the lower inset (b) is the Mn mapping after the MnOx-modification.

is modified with MnOx (30 or 60 potential cycles). This behavior can be understood in view of the competition between the electronic and geometric factors influencing the electrocatalytic activity of the electrode. As the loading of MnOx increases, an enhancement in the electrocatalytic activity of the electrode occurs based on the electronic influence. At the same time, the real surface area of the electrode decreases leading to a reduction in the electrode activity. Therefore, a MnOx loading of 15 cycles is recommended for the modification of S-Pt/TiOx (600) electrode.

Recalling the data in Table 2, we find that a negative potential shift of 228 mV was obtained for OER at the S-Pt/TiOx (600) electrode at 20 mA cm^{-2} in 0.5 M KOH if compared to the bare-Pt electrode. An extra cathodic shift of 242 mV was obtained under the same conditions on the S-Pt/TiOx(600) electrode after MnOx (15 cycles) modification. This means that a synergetic enhancement was obtained on the MnOx-modified S-Pt/TiOx(600) electrode with a total cathodic shift of 470 mV for OER in 0.5 M KOH at 20 mA cm^{-2}.

The Tafel plots were also measured to account for the charge transfer and mechanism of OER. Fig. 10 shows that the Tafel plots for the bare Pt electrode (Fig. 10a), S-Pt/TiOx(600) (Fig. 10b) and the S-Pt/TiOx(600) after modification with 15 cycles of MnOx (Fig. 10c) were all parallel to each other with a slope close to 120 mV/decade. The similarity of the Tafel slopes indicates that oxygen evolution proceeds via a common rate-determining step; water discharge. This behavior is quite analogous to those reported in literature (Mohammad et al., 2008; Sadiek et al., 2012; Al-Akraa et al., 2017). Furthermore, the apparent exchange current density of the OER at the S-Pt/TiOx(600) after modification with 15 cycles of MnOx (Fig. 10c) electrode was higher approximately by one order of magnitude than that estimated at the bare Pt electrode (Fig. 10a). This again supports the faster and favorable OER at the MnOx-modified electrode.

We expect that our investigation will attract attention toward the use of mixed manganese and titanium oxides modified catalysts in water electrolysis.

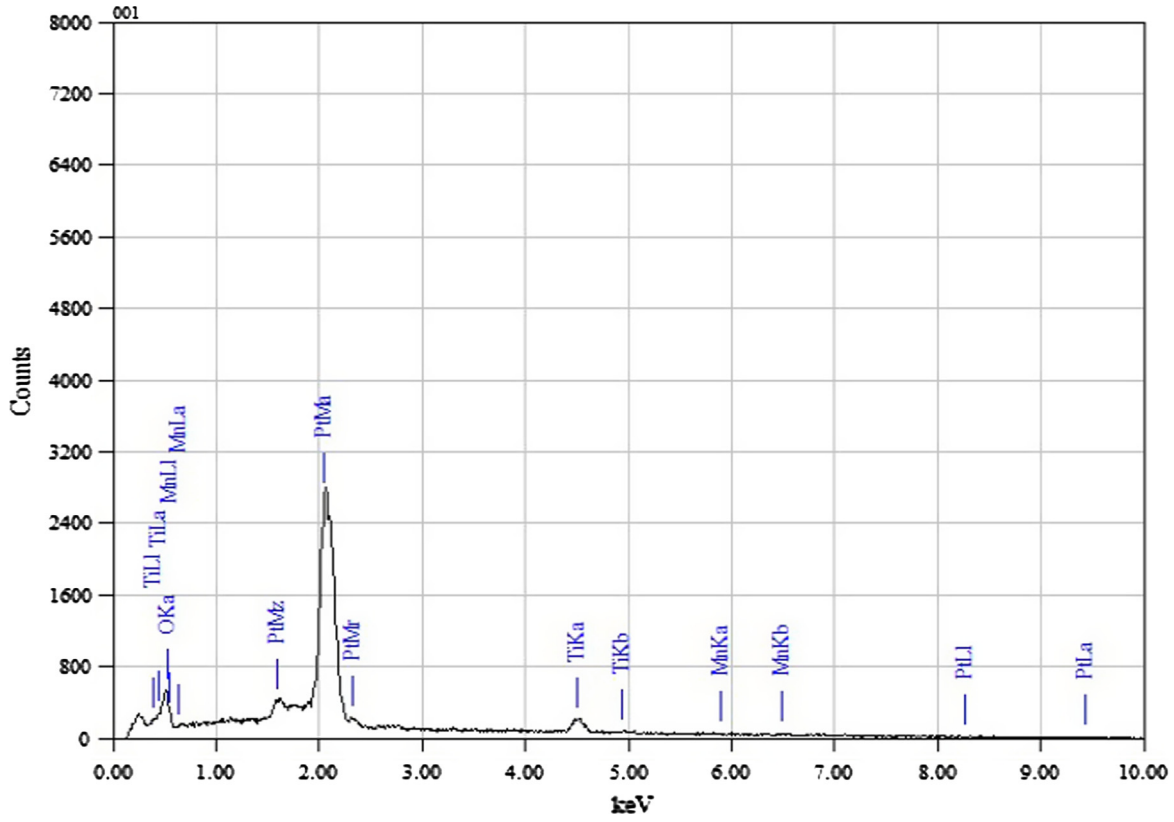

Fig. 8 The EDXS profile obtained for the S-Pt/TiOx(600) electrode after electrodepositing MnOx (15 potential cycles).

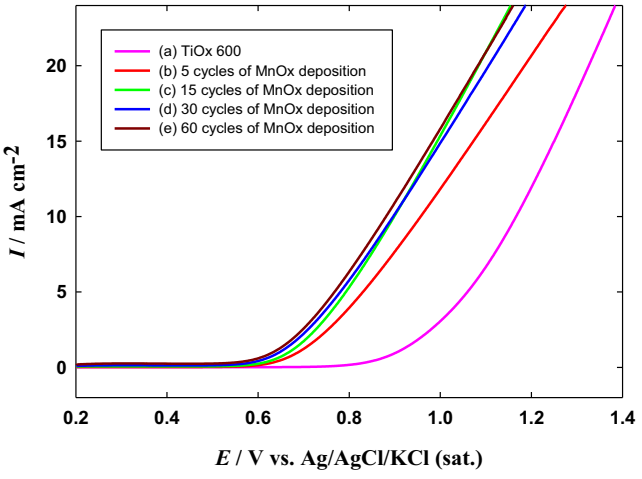

Fig. 9 The LSVs response for OER in N_2-saturated 0.5 M KOH solution at a potential scan rate of 5 mV s^{-1} for the spin-coated S-Pt/TiOx electrode annealed at 600 °C before (a) and after modification with MnOx. The MnOx was electrochemically deposited from an aqueous solution of 0.1 M Na_2SO_4 containing 0.1 M $Mn(CH_3COO)_2$ by applying 5 (b), 15 (c), 30 (d), 60 (e) potential cycles between 0 and 0.4 V vs. Ag/AgCl/KCl (sat.) at potential scan rate of 20 mV s^{-1}.

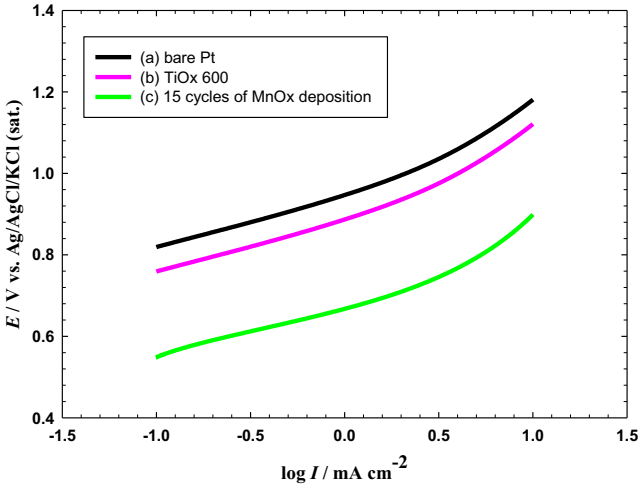

Fig. 10 Tafel plots for the OER in N_2-saturated 0.5 M KOH solution for the bare Pt electrode (a), S-Pt/TiOx(600) (b) and the S-Pt/TiOx(600) after modification with 15 cycles of MnOx (c).

4. Conclusion

An efficient S-Pt/TiOx electrode was recommended for the oxygen evolution reaction (OER). The catalytic performance of the electrode depended on its annealing temperature and the electrolyte's pH where annealing at 600 °C and working under highly basic condition appeared favorable for OER. A further modification of this S-Pt/TiOx(600) electrode with different loadings of MnOx resulted in a synergetic enhancement for OER with a cathodic shift of 470 mV for OER in 0.5 M KOH at 20 mA cm^{-2}. Analysis of the electrocatalytic activity showed that the main contribution comes from the electronic rather than geometric nature of the electrode.

Funding statement

This research was supported from the General Scientific Research Department at Cairo University (Grant 77/2016). Dr. Al-Akraa appreciate the financial support given from the British University in Egypt (Young Investigator Research Grant/YIRG2017-03).

Appendix A. Supplementary material

Supplementary data to this article can be found online at https://doi.org/10.1016/j.arabjc.2019.01.006.

References

Abdullah, A.M., Mohammad, A.M., Okajima, T., Kitamura, F., Ohsaka, T., 2009. Effect of load, temperature and humidity on the pH of the water drained out from H_2/air polymer electrolyte membrane fuel cells. J. Power Sources 190, 264–270.

Al-Akraa, I.M., Mohammad, A.M., El-Deab, M.S., El-Anadouli, B.E., 2017. Flower-shaped gold nanoparticles: Preparation, characterization, and electrocatalytic application. Arab. J. Chem. 10, 877–884.

Alfredo, U.A., 2012. Hydrogen production from water electrolysis: current status and future trends. Proc. IEEE 100, 410–426.

Bagotsky, V.S., 2006. Fundamentals of Electrochemistry. John Wiley & Sons Inc, New Jersey.

Balogun, M.-S., Qiu, W., Huang, Y., Yang, H., Xu, R., Zhao, W., Li, G.-R., Ji, H., Tong, Y., 2017. Cost-effective alkaline water electrolysis based on nitrogen- and phosphorus-doped self-supportive electrocatalysts. Adv. Mater. 29, 1702095.

Balogun, M.-S., Qiu, W., Yang, H., Fan, W., Huang, Y., Fang, P., Li, G., Ji, H., Tong, Y., 2016. A monolithic metal-free electrocatalyst for oxygen evolution reaction and overall water splitting. Energy Environ. Sci. 9, 3411–3416.

Bard, A.J., Faulkner, L.R., 2001. Electrochemical Methods: Fundamentals and Applications. John Wiley & Sons Inc, New York.

Battiston, G.A., Gerbasi, R., Porchia, M., Marigo, A., 1994. Influence of substrate on structural properties of TiO_2 thin films obtained via MOCVD. Thin Solid Films 239, 186–191.

Beni, G., Schiavone, L.M., Shay, J.L., Dautremont-Smith, W.C., Schneider, B.S., 1979. Electrocatalytic oxygen evolution on reactively sputtered electrochromic iridium oxide films. Nature 282, 281–283.

Boffa, A.B., Galloway, H.C., Jacobs, P.W., Benitez, J.J., Batteas, J.D., Salmeron, M., Bell, A.T., Somorjai, G.A., 1995. The growth and structure of titanium oxide films on Pt(111) investigated by LEED, XPS, ISS, and STM. Surf. Sci. 326, 80–92.

Cahen, G.L.J., Moran, P.J., Scribner, L.L., Stoner, G.E., 1981. Investigation of nickel whiskers networks as electrodes for hydrogen and oxygen evolution. J. Electrochem. Soc. 128, 1877–1880.

Chakik, F.E., Kaddami, M., Mikou, M., 2017. Effect of operating parameters on hydrogen production by electrolysis of water. Int. J. Hydrogen Energy 42, 25550–25557.

Cherevko, S., Geiger, S., Kasian, O., Mingers, A., Mayrhofe, J.J., 2016. Oxygen evolution activity and stability of iridium in acidic media. Part 2. –Electrochemically grown hydrous iridium oxide. J. Electroanal. Chem. 774, 102–110.

De Faria, L.A., Boodts, J.F.C., Trasatti, S., 1996. Electrocatalytic properties of ternary oxide mixtures of composition $Ru_{0.3}Ti_{(0.7-x)}Ce_xO_2$: Oxygen evolution from acidic solution. J. Appl. Electrochem. 26, 1195–1199.

El-Deab, M.S., Awad, M.I., Mohammad, A.M., Ohsaka, T., 2007. Enhanced water electrolysis: Electrocatalytic generation of oxygen gas at manganese oxide nanorods modified electrodes. Electrochem. Commun. 9, 2082–2087.

El-Deab, M.S., El-Nagar, G.A., Mohammad, A.M., El-Anadouli, B. E., 2015. Fuel blends: Enhanced electro-oxidation of formic acid in its blend with methanol at platinum nanoparticles modified glassy carbon electrodes. J. Power Sources 286, 504–509.

Guo, X., Zheng, T., Ji, G., Hu, N., Xu, C., Zhang, Y., 2018. Core/shell design of efficient electrocatalysts based on $NiCo_2O_4$ nanowires and NiMn LDH nanosheets for rechargeable zinc–air batteries. J. Mater. Chem. A 6, 10243–10252.

Han, G.-Q., Liu, Y.-R., Hu, W.-H., Dong, B., Li, X., Shang, X., Chai, Y.-M., Liu, Y.-Q., Liu, C.-G., 2015. Three dimensional nickel oxides/nickel structure by in situ electro-oxidation of nickel foam as robust electrocatalyst for oxygen evolution reaction. Appl. Surf. Sci. 359, 172–176.

Kim, J.-H., Ishihara, A., Mitsushima, S., Kamiya, N., Ota, K.-I., 2007. Catalytic activity of titanium oxide for oxygen reduction reaction as a non-platinum catalyst for PEFC. Electrochim. Acta 52, 2492–2497.

Koryta, J., Dvorak, W., Kavan, L., 1993. Principles of Electrochemistry. John Wiley & Sons Ltd., Chichester, England.

Koyama, H., Fujimoto, M., Ohno, T., Suzuki, H., Tanaka, J.A.C.S., 2006. Effects of thermal annealing on formation of micro porous titanium oxide by the sol-gel method. J. Am. Ceram. Soc. 89, 3536–3540.

Lee, K.-S., Park, I.-S., 2003. Anatase-phase titanium oxide by low temperature oxidation of metallic Ti thin film. Scr. Mater. 48, 659–663.

Li, M., Liu, T., Bo, X., Zhou, M., Guo, L., Guo, S., 2017. Hybrid carbon nanowire networks with Fe–P bond active site for efficient oxygen/hydrogen-based electrocatalysis. Nano Energy 33, 221–228.

Li, Y.-Q., Fu, S.-Y., Yang, G., Li, M., 2006. Preparation and characterization of a novel solid titania precursor. J. Non-Cryst. Solids 352, 3339–3342.

Liu, T., Li, M., Bo, X., Zhou, M., 2018a. Comparison study toward the influence of the second metals doping on the oxygen evolution activity of cobalt nitrides. ACS Sustain. Chem. Eng. 6, 11457–11465.

Liu, T., Li, M., Dong, P., Zhang, Y., Guo, L., 2018b. Design and facile synthesis of mesoporous cobalt nitride nanosheets modified by pyrolytic carbon for the nonenzymatic glucose detection. Sens. Actuators B Chem. 255, 1983–1994.

Liu, T., Li, M., Su, Z., Bo, X., Guan, W., Zhou, M., 2018c. Monodisperse and tiny $Co_2N_{0.67}$ nanocrystals uniformly embedded over two curving surfaces of hollow carbon microfibers as efficient electrocatalyst for oxygen evolution reaction. ACS Appl. Nano Mater. 1, 4461–4473.

Malevich, D.V., Drozdovich, V.B., Zharskii, I.M., 1997. Studies in surface science and catalysis. Stud.surf. sci. catal. 112, 359–366.

Marino, C.E.B., Nascente, P.A.P., Biaggio, S.R., Rocha-Filho, R.C., Bocchi, N., 2004. XPS characterization of anodic titanium oxide films grown in phosphate buffer solutions. Thin Solid Films 468, 109–112.

Mentus, S.V., 2004. Oxygen reduction on anodically formed titanium dioxide. Electrochim. Acta 50, 27–32.

Mohammad, A.M., Al-Akraa, I.M., El-Deab, M.S., 2018. Superior electrocatalysis of formic acid electro-oxidation on a platinum, gold and manganese oxide nanoparticle-based ternary catalyst. Int. J. Hydrogen Energy 43, 139–149.

Mohammad, A.M., Awad, M.I., El-Deab, M.S., Okajima, T., Ohsaka, T., 2008. Electrocatalysis by nanoparticles: Optimization of the loading level and operating pH for the oxygen evolution at crystallographically oriented manganese oxide nanorods modified electrodes. Electrochim. Acta 53, 4351–4358.

Mohammad, A.M., El-Nagar, G.A., Al-Akraa, I.M., El-Deab, M.S., El-Anadouli, B.E., 2015. Towards improving the catalytic activity and stability of platinum-based anodes in direct formic acid fuel cells. Int. J. Hydrogen Energy 40, 7808–7816.

Mohammad, A.M., Kitsuka, K., Abdullah, A.M., Awad, M.I., Okajima, T., Kaneda, K., Ikematsu, M., Ohsaka, T., 2009.

Development of spin-coated Si/TiOx/Pt/TiOx electrodes for the electrochemical ozone production. Appl. Surf. Sci. 255, 8458–8463.
Mohammad, A.M., Kitsuka, K., Kaneda, K., Awad, M.I., Abdullah, A.M., Ikematsu, M., Ohsaka, T., 2007. Superior electrocatalysis of spin-coated titanium oxide electrodes for the electrochemical ozone production. Chem. Lett. 36, 1046–1047.
Nam, W., Han, G.Y., 2007. Preparation and characterization of anodized Pt-TiO_2 nanotube arrays for water splitting. J. Chem. Eng. Jpn. 40, 266–269.
Osgood, H., Devaguptapu, S.V., Xu, H., Cho, J., Wu, G., 2016. Transition metal (Fe Co, Ni, and Mn) oxides for oxygen reduction and evolution bifunctional catalysts in alkaline media. Nano Today 11, 601–625.
Pan, L., Zhu, X.-D., Xie, X.-M., Liu, Y.-T., 2015. Smart hybridization of TiO_2 nanorods and Fe_3O_4 nanoparticles with pristine graphene nanosheets: hierarchically nanoengineered ternary heterostructures for high-rate lithium storage. Adv. Funct. Mater. 25, 3341–3350.
Paoli, E.A., Masini, F., Frydendal, R., Deiana, D., Malacrida, P., Hansen, T.W., Chorkendorff, I., Stephens, I.E.L., 2016. Fine-tuning the activity of oxygen evolution catalysts: The effect of oxidation pre-treatment on size-selected Ru nanoparticles. Catal. Today 262, 57–64.
Park, E.J., Capuano, C.B., Ayers, K.E., Bae, C., 2018. Chemically durable polymer electrolytes for solid-state alkaline water electrolysis. J. Power Sources 375, 367–372.
Sadiek, I.M., Mohammad, A.M., El-Shakre, M.E., El-Deab, M.S., 2012. Electrocatalytic activity of nickel oxide nanoparticles-modified electrodes: Optimization of the loading level and operating pH towards the oxygen evolution reaction. Int. J. Hydrogen Energy 37, 68–77.
Santana, M.H.P., De Faria, L.A., 2006. Oxygen and chlorine evolution on RuO_2 + TiO_2 + CeO_2 + Nb_2O_5 mixed oxide electrodes. Electrochim. Acta 51, 3578–3585.
Selvaraj, U., Prasadarao, A.V., Komarneni, S., Roy, R., 1992. Sol-gel fabrication of expitaxial and oriented TiO_2 thin films. J. Am. Ceram. Soc. 75, 1167–1170.
Tahir, M., Pan, L., Idrees, F., Zhang, X., Wang, L., Zou, J.-J., Wang, Z.L., 2017. Electrocatalytic oxygen evolution reaction for energy conversion and storage: A comprehensive review. Nano Energy 37, 136–157.
Takagi, K., Makimoto, T., Hiraiwa, H., Negishi, T., 2001. Photocatalytic, antifogging mirror. J. Vac. Sci. Technol., A 19, 2931–2935.
Tokarev, A.V., Kustov, L.M., Ivaska, A., Murzin, D.Y., 2006. Cyclic voltammetry as a tool for characterization of supported VIII group metal catalysts. Appl. Catal. A 309, 52–61.
Trasatti, S., Petrii, O.A., 1991. Real surface area measurements in electrochemistry. Pure Appl. Chem. 63, 711–734.
Wang, F., Liu, Z.-B., Wang, K.-X., Zhu, X.-D., Fan, X.-H., Gao, J., Feng, Y.-J., Sun, K.-N., Liu, Y.-T., 2018. Dandelion-like Co_3O_4 mesoporous nanostructures supported by a Cu foam for efficient oxygen evolution and lithium storage. Chem. Commun. 54, 5138–5141.
Wang, J., 2006. Analytical Electrochemistry. John Wiley & Sons Inc, Hoboken, New Jersey.
Wang, R., Hashimoto, K., Fujishima, A., Chikuni, M., Kojima, E., Kitamura, A., Shimohigoshi, M., Watanabe, T., 1998. Photogeneration of Highly Amphiphilic TiO_2 Surfaces. Adv. Mater. 10, 135–138.
Xu, W., Jiang, Z., Yang, Q., Huo, W., Javed, M.S., Li, Y., Huang, L., Gu, X., Hu, C., 2018a. Approaching the lithium-manganese oxides' energy storage limit with Li_2MnO_3 nanorods for high-performance supercapacitor. Nano Energy 43, 168–176.
Xu, W., Lu, J., Huo, W., Li, J., Wang, X., Zhang, C., Gu, X., Hu, C., 2018b. Direct growth of $CuCo_2S_4$ nanosheets on carbon fiber textile with enhanced electrochemical pseudocapacitive properties and electrocatalytic properties towards glucose oxidation. Nanoscale 10, 14304–14313.
Yao, W., Yang, J., Wang, J., Nuli, Y., 2007. Chemical deposition of platinum nanoparticles on iridium oxide for oxygen electrode of unitized regenerative fuel cell. Electrochem. Commun. 9, 1029–1034.
Yoko, T., Yuasa, A., Kamiya, K., Sakka, S., 1991. Sol-Gel-Derived TiO_2 Film Semiconductor Electrode for Photocleavage of Water: Preparation and Effects of Postheating Treatment on the Photoelectrochemical Behavior. J. Electrochem. Soc. 138, 2279–2285.
Zheng, J., 2017. Binary platinum alloy electrodes for hydrogen and oxygen evolutions by seawater splitting. Appl. Surf. Sci. 413, 72–82.
Zhu, S., Li, L., Liu, J., Wang, H., Wang, T., Zhang, Y., Zhang, L., Ruoff, R.S., Dong, F., 2018a. Structural directed growth of ultrathin parallel birnessite on β-MnO_2 for high-performance asymmetric supercapacitors. ACS Nano 12, 1033–1042.
Zhu, X.-D., Xie, Y., Liu, Y.-T., 2018b. Exploring the synergy of 2D MXene-supported black phosphorus quantum dots in hydrogen and oxygen evolution reactions. J. Mater. Chem. A 6, 21255–21260.